Frontiers in Heat and Mass Transfer (FHMT), 12, 9 (2019)
DOI: 10.5098/hmt.12.9

Global Digital Central
ISSN: 2151-8629

Frontiers in Heat and Mass Transfer

Available at www.ThermalFluidsCentral.org

EXERGY ANALYSIS IN ENERGY SYSTEMS: FUNDAMENTALS AND APPLICATION

Hamidreza Shabgard[a,*], Amir Faghri[b]

[a] *School of Aerospace and Mechanical Engineering, University of Oklahoma, Norman, OK 73019, USA*
[b] *Department of Mechanical Engineering, University of Connecticut, Storrs, CT 06269, USA*

ABSTRACT

Fundamentals of exergy analysis in energy systems are reviewed and presented in a cohesive and general manner for the study of energy systems. The exergy analysis is applied to several engineering systems and processes, namely fuel cells, latent heat thermal energy storage, heat exchangers and thermal desalination systems to obtain insight on the best optimization strategies as well as the theoretical limits of performance. The various sources of irreversibility and optimal operating conditions are presented for relevant applications. It is also shown that for some systems the exergy efficiency as a function of a given parameter may have opposite trend than the first law efficiency.

Keywords: *Exergy analysis, Energy systems, Engineering application*

1. INTRODUCTION

Design and optimization of energy systems based solely upon the energy analysis derived from the first law of thermodynamics may lead to deceiving results. Exergy analysis combines the first and second laws of thermodynamics in order to provide a better understanding of the actual level of performance with respect to the theoretical and practical limits. In general, the efficiency of a system which consumes some resources to deliver a certain functionality can be defined as:

$$\eta_I = \frac{\text{Useful effect}}{\text{Provided input}} \tag{1}$$

This ratio provides a simple and easily understandable idea of how well the considered machine uses the provided input to accomplish its task. Using the first law of thermodynamics it is possible to determine all the required information about the energy balance of the system. However, by focusing on the energy balance alone, the difference between the "quality" of the input and output energies of the system are not taken into account (Galliani and Pedrocchi, 2014).

A common example considers a lake containing an enormous amount of thermal energy. However, the thermal energy has negligible potential for producing work. The reason for this is that according to the second law of thermodynamics if a system is to produce work from a source of thermal energy it must also be in thermal communication with a heat sink. Since the lake is at the same temperature as the environment, its thermal energy content is not exploitable using the environment itself as a heat sink. This example sheds light on the concept of quality of thermal energy: the greater the temperature difference between a certain medium and its heat sink, the greater the potential for its thermal energy to produce work. The relation between the temperatures of the hot and cold media, T_h and T_c, respectively, and the potential for delivering useful work is explained by the Carnot efficiency, which sets the limit to the maximum first law efficiency of a cycle operating between two temperatures (Çengel *et al.*, 2019; Moran *et al.*, 2014):

$$\eta_{Carnot} = 1 - \frac{T_c}{T_h} \tag{2}$$

For a heat source and heat sink at known temperatures, the Carnot efficiency defines the maximum amount of work that is possible to derive and the corresponding heat transfer. Thus, a precise definition of the lower temperature limit, or more generally, the definition of all the properties of the environment which serves as the ultimate heat sink is extremely important.

Considering that the majority of engineering systems are exposed to atmospheric conditions, it is reasonable to assume atmospheric conditions (temperature, pressure, chemical composition, etc.) as the final equilibrium state, at which all driving forces have been exploited and a system is not able to produce more work. The state at which a system is in complete equilibrium (thermal, mechanical and chemical) with the environment is defined as the dead state, for which the standard temperature and pressure values are often assumed to be T_0 = 25°C and p_0 = 1 atm (the chemical composition of the dead state will be discussed later). It is noted that the properties of the dead state are not influenced by the processes that take place in the environment and can be considered constant.

For a general system at certain conditions it would be helpful to establish the maximum amount of work that can be obtained by bringing it to equilibrium with the environment, or dead state. Second law of thermodynamics asserts that among all the processes that take a system from state *A* to state *B* a reversible process with no entropy generation yields the maximum work. Thus, a new property, namely exergy, can be defined as the amount of work obtained by bringing a system from its current state to the dead state through a reversible process. Exergy proves to be a very powerful tool in analyzing performances, not only for devices that produce work, but also for those that require work to accomplish certain tasks. A practical application in which exergy analysis gives a much better measure of performance than the energy-based efficiency is geothermal power generation. Typically, the temperature difference between the geothermal well and the environment

* *Corresponding author. Email: shabgard@ou.edu*

Global Digital Central
ISSN: 2151-8629

is relatively small, and the first law efficiency of a power plant using geothermal heat for electricity generation may be limited to 10-15%. The relatively small efficiency does not mean that the power plant is poorly designed; its efficiency might be very close to the thermodynamic limit (Carnot efficiency), but the first law does not accurately describe the actual level of its performance. However, if the exergy associated with the well is determined, the actual power generation can be compared with the maximum power production capacity to assess the quality of the design and to identify the main causes of inefficiency.

Review of the literatures shows that there are numerous publications focusing on the fundamentals and applications of the exergy analysis in engineering systems. Some recent related publications are listed in Table 1.

Table 1 Representative recent publications on the fundamentals and applications of the exergy analysis.

Author, year	**Approach and Scope**	**Highlights**	**Main Conclusions**
Pavelka *et al.* (2015)	Approach: Analytical Scope: - Describing classical exergy analysis - Proposing new method of exergy analysis	- Standard exergy analysis is argued to show the maximum available work as a function of all energy fluxes except for heat flux from the environment at temperature T_0. - Generalization of exergy analysis using classical irreversible thermodynamics was derived for fuel cells, osmotic power plant and heat engines. - General algorithm of thermodynamic optimization presented.	- It was argued that in some cases some classical exergy analysis and entropy minimization does not lead to maximizing the work potential. - General algorithm for thermodynamic optimization was formulated which is applicable in cases where the classical analysis does not yield useful results.
Kaushik *et al.*, (2011)	Approach: Analytical, review Scope: - Classical exergy analysis - Comparison based on energy and exergy analysis between coal and gas fired power plants	- First and second law analysis applied for the coal fired power plant as well as gas fired combined cycle power plants.	- Performing exergetic and energetic analyses together can give a complete depiction of system characteristics. - Boiler and combustion chamber were identified as the main sources of exergy losses in coal and combined cycle power plants, respectively.
Fallah *et al.*, (2016)	Approach: Analytical, numerical (EES) Scope: Classical exergy analysis, proposing advanced exergy analysis (showing external and internal sources of irreversibilities)	- Drawing a comprehensive comparison between four different gas turbines: simple gas turbine (SGT), gas turbine with evaporative inlet air cooler (EVGT), steam injection gas turbine (STIG) and steam injection gas turbine with evaporative inlet air cooler (ESTIG). - Conventional energy and exergy analysis of ESTIG conducted and compared with the	- The ESTIG is found to provide the greatest amount of work, as well as first law and second law efficiencies - Advanced exergy analysis of ESTIG showed that at the maximum net work condition, the combustion chamber has the highest exergy destruction rate (and optimization priority), followed by the HRSG, the
		proposes exergy analysis - Engineering equation solver (EES) software used for simulation and for calculation of the characteristic parameters of the systems	turbine, and the compressor.
Ibrahim *et al.*, (2018)	Approach: Analytical, review Scope: Classical exergy analysis, energy analysis	- Thermodynamic energy and exergy analysis derived for Combined cycle power plant - Analysis applied to three case study power plants, namely externally-fired biomass, combined cycle, and dual pressure combined cycle power plant	- Combination of energy and exergy analysis improved the system performance assessment in a way that was not attainable by just energy analysis - Energy losses during operation can be large. However, thermodynamically the effect of this lost energy is negligible due to its low quality.
Sansaniwal *et al.*, (2018)	Approach: Analytical, review Scope: Classical thermodynamic energy and exergy analysis.	- General relations for a steady flow process derived by using balance equations in order to find the energy and exergy efficiencies. - Exergy improvement potential examined - Thermodynamic functions such as fuel depletion ratio, relative irreversibility, productivity lack and exergetic factor considered in the exergy analysis. - Energy and exergy analysis performed for various solar energy applications (solar drying, solar air conditioning and refrigeration, solar water heating, solar cooking and solar power generation through solar photovoltaic and concentrated solar power)	- The energy efficiency was found to be greater than the exergy efficiency. - The energy and exergy efficiencies are highly dependent on the intensity of solar radiations on daily basis. - Thermal energy storage improves the energetic and exergetic performance of various solar energy systems.
Pal, (2018)	Approach: Analytical, experimental Scope: -Entropy generation and exergy destruction associated with various fluid flows. - Quantification of exergy destruction in flows of	- Entropy balance alongside with momentum and energy balance equations for fluid flow derived. - Exergy destruction in fluid flow studied using the Gouy-Stodola theorem - Experiment conducted to evaluate exergy destruction for two-phase and multiphase dispersions - Exergy destruction in three-phase blends was	- The exergy destruction rate in flow of emulsions of oil droplets and polymeric matrix did not change significantly with the increase in the concentration of oil droplets - The exergy destruction rate in flow of suspensions of solid particles and polymeric matrix increased with the

Global Digital Central
ISSN: 2151-8629

	emulsions, suspensions and blends of emulsion and suspensions	found to be a unique function of concentration of solid particles	increase in particle concentration
Torabi *et al.*, (2016)	Approach: Analytical, review Scope: Classical thermodynamic, Entropy generation and exergy destruction	- Entropy generation was studied in thermal systems with conductive parts - Local entropy generation rate was determined by assuming one-dimensional heat transfer - Entropy generation and exergy destruction in various thermal system with solid part (pure conductive media, conjugate heat transfer systems, porous media, and thermoelectric systems) was reviewed. - Four solution methodologies for the heat transfer problem are reviewed, namely, exact analytical, approximate analytical, numerical simulation and combined analytical-numerical techniques	- A relatively new technological manifestation of conduction dominated processes was reported in thermoelectric devices - Combined analytical-numerical and the numerical methods were identified as the techniques that offer the most attractive features for the foreseeable future of entropy generation modeling
Boroumand Jazi *et al.*, (2012)	Approach: Analytical, review Scope: Classical thermodynamic exergy and energy analysis, review on technical characteristics.	- Exergy analysis was utilized to determine the maximum performance of renewable energy systems and their irriversibilities -The reliability of a system, defined as the probability of a system being inoperable due to an unscheduled event, was studied based on the exergy efficiency of the system - Sustainability was investigated as another characteristic of the system using the sustainability index, defined as the relation between sustainable development and exergy	- Investigating the reliability and sustainability of the renewable energy systems can convince the importance of utilizing them versus their high initial cost - The sustainable systems, which have less environmental impact, have the higher energy and exergy efficiencies

Despite the great amount of effort made on the development of second law analysis and its application to engineering systems, most of the available work is focused on a specific application. To this end, the present work aims to provide a cohesive and general approach for the study of energy systems based on the second law of thermodynamics with an emphasis on exergy analysis. The developed second law metrics, particularly the exergy efficiency, are used to evaluate the performance of some familiar and important energy systems and processes widely used in engineering applications. Also, the role of second law analysis in identification of the sources of irreversibility in engineering systems is demonstrated in practical applications.

2. THERMODYNAMIC ANALYSIS

This section is focused on the analysis of general exergy balance for a system, beginning with examination of various forms of energy and their potential to produce work, and followed by derivation of the expressions for the exergy of ideal gases and incompressible material in special cases of constant temperature and constant pressure.

All forms of mechanical energy have the same thermodynamic quality of work. That is, ideally, kinetic and potential energy can be entirely converted to work without any thermodynamic limitation. Hence, the exergy associated with a certain amount of mechanical energy is equivalent to the amount of the energy itself. This will be proved false for internal energy and enthalpy. The equivalent exergy for the kinetic and potential energies, respectively, are:

$$X_{ke} = m x_{ke} = KE = m \frac{V^2}{2} \tag{3}$$

$$X_{pe} = m x_{pe} = PE = m\, g\, h \tag{4}$$

where V shows the velocity, h is the displacement against gravity, and X and x are the total and specific (per unit mass) exergy, respectively. Equations (3) and (4) can be written in a rate basis:

$$\dot{X}_{ke} = \dot{m}\, x_{ke} = \dot{m}\, \frac{V^2}{2} \tag{5}$$

$$\dot{X}_{pe} = \dot{m}\, x_{pe} = \dot{m}\, g\, h \tag{6}$$

The exergy of other forms of energy is examined using a control volume exchanging mass, thermal energy, and work with its surroundings (Fig. 1). It is assumed that no chemical reaction takes place in the control volume (chemical exergy will be analyzed in detail later). Also, potential and kinetic energies will be neglected. The control volume receives heat $\dot{Q}_1$ to $\dot{Q}_n$ from sources at temperatures T_1 to T_n, respectively, while rejecting heat $\dot{Q}_0$ to the environment at T_0 and p_0. The work produced by the control volume is represented by $\dot{W}$, and $\dot{m}_{in}$ and $\dot{m}_{out}$ are the total mass flow rates entering and exiting the system, respectively. All quantities are positive when entering the control volume.

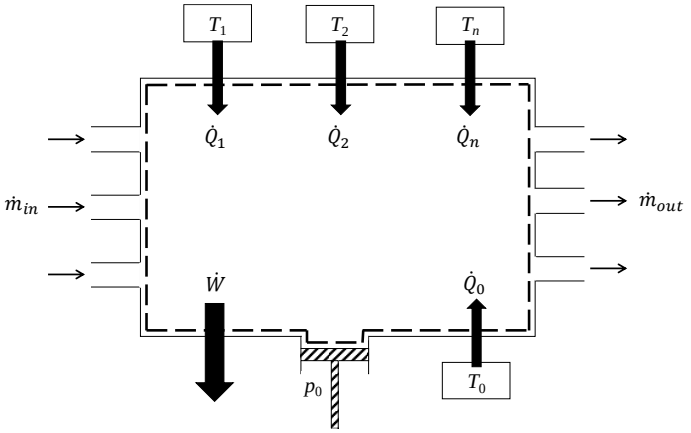

Fig. 1 Representative control volume exchanging mass, heat and work with surroundings

The energy and entropy balances for the control volume can be written as following, respectively (Dinçer and Rosen, 2012):

$$\frac{dU}{dt} = \sum_{in} \dot{m}_i\, h_i - \sum_{out} \dot{m}_o\, h_o + \sum_n \dot{Q}_n + \dot{Q}_0 - \dot{W} - p_0 \frac{dV}{dt} \tag{7}$$

$$\frac{dS}{dt} = \sum_{in} \dot{m}_i\, s_i - \sum_{out} \dot{m}_o\, s_o + \sum_n \frac{\dot{Q}_n}{T_n} + \frac{\dot{Q}_0}{T_0} + \dot{S}_{gen} \tag{8}$$

where U, S and V are the total internal energy, entropy, and volume of the system, and h and s show the specific enthalpy and specific entropy,

Global Digital Central
ISSN: 2151-8629

respectively. Substituting $\dot{Q}_0$ from Eq. (8) into Eq. (7) and rearranging Eq. (7) in terms of $\dot{W}$ yields:

$$\dot{W} = -\left(\frac{dU}{dt} + p_0\,\frac{dV}{dt} - T_0\,\frac{dS}{dt}\right) + \sum_{in} \dot{m}_i\,(h_i - T_0\,s_i) - \sum_{out} \dot{m}_o\,(h_o - T_0\,s_o) + \sum_n \dot{Q}_n\left(1 - \frac{T_0}{T_n}\right) - T_0\,\dot{S}_{gen} \quad (9)$$

To simplify Eq. (9), the following terms are introduced:

$$U^a = U + p_0\,V - T_0\,S;\ \text{available internal energy or co-energy} \quad (10)$$

$$h^a = h - T_0\,s;\ \text{available specific enthalpy or co-enthalpy} \quad (11)$$

$$\vartheta_n = 1 - \frac{T_0}{T_n};\ \text{Carnot factor} \quad (12)$$

Using Eqs. (10) to (12), Eq. (9) can be rewritten as:

$$\dot{W} = -\frac{dU^a}{dt} + \sum_{in} \dot{m}_i\,h_i^a - \sum_{out} \dot{m}_o\,h_o^a + \sum_n \dot{Q}_n\,\vartheta_n - T_0\,\dot{S}_{gen} \quad (13)$$

where the product $\dot{Q}_n\,\vartheta_n$ represents the maximum amount of work that can be obtained by exploiting the heat $\dot{Q}_n$ available at a given temperature T_n using a Carnot cycle operating between T_n and T_0. The *thermal exergy* $\dot{X}_{th}$ associated with thermal energy $\dot{Q}$ delivered at temperature T is defined as:

$$\dot{X}_{th} = \dot{Q}\,\vartheta = \dot{Q}\,(1 - \frac{T_0}{T}) \quad (14)$$

Regarding co-energy and co-enthalpy, it is of interest to evaluate their change with respect to the dead state. To do so, the Eq. (13) is applied to an adiabatic open system in equilibrium with dead state with multiple mass inlets and outlets (exchanging mass with the environment at dead state) and no irreversibilities. For such a system, the last two terms on the right-hand side of Eq. (13) vanish. Since the energy of this system does not change with time (the system is at equilibrium with its environment), the time variations of co-energy due to the component *j* can be expressed as:

$$\frac{dU_{j,0}^a}{dt} = \frac{d\left(m_j\,u_{j,0}^a\right)}{dt} = u_{j,0}^a\,\frac{dm_j}{dt} = \left(u_{j,0} + p_0 v_{j,0} - T_0 s_{j,0}\right)\frac{dm_j}{dt} \quad (15)$$

where the subscript "0" stands for "at dead state" for each (j^{th}) component of the system. Also, the co-enthalpy for the j^{th} component at the system boundary can be written as:

$$h_{j,0}^a = h_{j,0} - T_0\,s_{j,0} = u_{j,0} + p_0 v_{j,0} - T_0 s_{j,0} \quad (16)$$

Substituting Eqs. (15) and (16) into the first three terms on the right-hand side of Eq. (13) yields:

$$\dot{W}_{j,0} = -\left(u_{j,0} + p_0 v_{j,0} - T_0 s_{j,0}\right)\left(\frac{dm_j}{dt} - \dot{m}_{j,in} + \dot{m}_{j,out}\right) = 0 \quad (17)$$

which is equal to zero due to the conservation of mass. Applying Eq. (17) for all the system components, the following equation is obtained:

$$\frac{dU_0^a}{dt} - \sum_{in} \dot{m}_{j,in}\,h_0^a + \sum_{out} \dot{m}_{j,out}\,h_0^a = 0 \quad (18)$$

Equation (18) can be added to Eq. (13) to obtain the potential of the system for generating work based on its departure from the dead state:

$$\dot{W} = -\frac{d(U^a - U_0^a)}{dt} + \sum_{in} \dot{m}_{j,in}\,(h^a - h_0^a)_{j,in} - \sum_{out} \dot{m}_{j,out}\,(h^a - h_0^a)_{j,out} + \sum_n \dot{Q}_n\,\vartheta_n - T_0\,\dot{S}_{gen} \quad (19)$$

It is evident in this expression that instead of having absolute values for co-energy and co-enthalpy, their change with respect to the dead state matters. The first term on the right-hand side of Eq. (19) shows the work potential of the internal energy of the system, while the combination of the second and third terms show the work potential of the net flow through the control volume and the last term shows the work potential of the net heat transferred across the system boundaries. Thus, two other types of exergy are identified: the *internal exergy*, X_{system}, and the *specific flow exergy*, x_{flow}:

$$X_{system} = U^a - U_0^a = (U - U_0) + p_0\,(V - V_0) - T_0\,(S - S_0) \quad (20)$$

$$x_{flow} = \psi = h^a - h_0^a = (h - h_0) - T_0\,(s - s_0) \quad (21)$$

For a reversible process, the entropy generation term, $\dot{S}_{gen}$, is zero and the work generation potential is maximized, implying that the term $T_0\,\dot{S}_{gen}$ can be associated with the loss in the potential work that the system is able to deliver, or in other words, a loss in exergy.

$$T_0\,\dot{S}_{gen} = \dot{W}_{loss} = \dot{X}_{des} \quad (22)$$

It also means that all other terms on the right-hand side of Eq. (19) represent the maximum amount of work that can be supplied by the system in a reversible process (with all boundary conditions fixed):

$$\dot{W} = \dot{W}_{rev} - T_0\,\dot{S}_{gen} = \dot{W}_{rev} - \dot{W}_{loss} \quad (23)$$

Rewriting this equation in terms of exergy components yields:

$$\dot{W} = -\frac{dX_{system}}{dt} + \sum \dot{m}_{j,in}\,\psi_{j,in} - \sum \dot{m}_{j,out}\,\psi_{j,out} + \sum_n \dot{X}_{th,n} - \dot{X}_{des} \quad (24)$$

If variations of the potential and kinetic energy cannot be neglected, the appropriate terms need to be added to the exergy balance equation. The exergy balance for a general system can now be expressed as:

$$\dot{W} = -\frac{dX_{system}}{dt} + \frac{d\left(X_{ke} + X_{pe}\right)_{system}}{dt} + \sum \dot{m}_{j,in}\left(\psi + x_{ke} + x_{pe}\right)_{j,in} - \sum \dot{m}_{j,out}\left(\psi + x_{ke} + x_{pe}\right)_{j,out} + \sum_n \dot{X}_{th,n} - \dot{X}_{des} \quad (25)$$

In the following, each of the terms appearing in Eq. (25) are described separately.

2.1 Internal Exergy

The exergy balance for a closed system (Fig. 2) with negligible kinetic and potential energy which thermally communicates only with the environment (the system interface with the environment is at the environment temperature) simplifies to:

$$\dot{W} = -\frac{dX_{system}}{dt} - \dot{X}_{des} = -\frac{d(U^a - U_0^a)}{dt} - \dot{X}_{des} \quad (26)$$

Integrating between an initial state and the final dead state yields:

$$W = U^a - U_0^a - X_{des} = X_{system} - X_{des} \quad (27)$$

where X_{system} shows the amount of work delivered by a closed system that exchanges heat only with its environment through a reversible process ($S_{gen} = X_{des} = 0$):

$$X_{system} = W_{rev} = (U - U_0) + p_0\,(V - V_0) - T_0\,(s - s_0) \quad (28)$$

Internal exergy of ideal gases:
For an ideal gas, internal energy and entropy are described by the following equations, respectively:

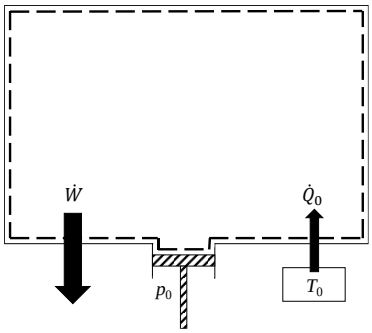

Fig. 2 Closed system with negligible kinetic and potential energy in thermal communication with the environment

$$u - u_0 = c_v\,(T - T_0) \tag{29}$$

$$s - s_0 = c_p\,\ln\frac{T}{T_0} - R_g\,\ln\frac{p}{p_0} \tag{30}$$

The volume of an ideal gas can be expressed in terms of temperature and pressure using the equation of state:

$$pV = mR_gT \tag{31}$$

Using Eqs. (29) to (31), Eq. (28) can be expressed as following:

$$X_{system,ig} = m\,c_v\,T_0\left(\frac{T}{T_0} - 1 - \frac{c_p}{c_v}\ln\frac{T}{T_0}\right) + R_g\,m\,T_0\left[\left(\frac{T}{T_0}\right)\left(\frac{p_0}{p}\right) - 1 - \ln\frac{p_0}{p}\right] \tag{32}$$

where $X_{system,ig}$ is the internal exergy of an ideal gas, and as evident, is a function of temperature and pressure only. It is of interest to examine the separate contributions of temperature and pressure to internal exergy of an ideal gas. For a constant temperature T_0, Eq. (32) yields the internal exergy of an ideal gas as a function of pressure only:

$$X_{system,ig}(T_0, p) = R_g\,m\,T_0\left[\frac{p_0}{p} - 1 - \ln\frac{p_0}{p}\right] \tag{33}$$

Figure 3 shows the internal exergy of an ideal gas (air) as a function of pressure at a constant temperature T_0. The curve has an asymptote as p approaches zero. For $0 < p < p_0$ there is a large change in internal exergy for small variations of p. For large pressure values ($p >> p_0$) the term p_0/p approaches zero and the logarithmic term dominates. When the gas is at the dead state (T_0, p_0), the exergy goes to zero, as expected.

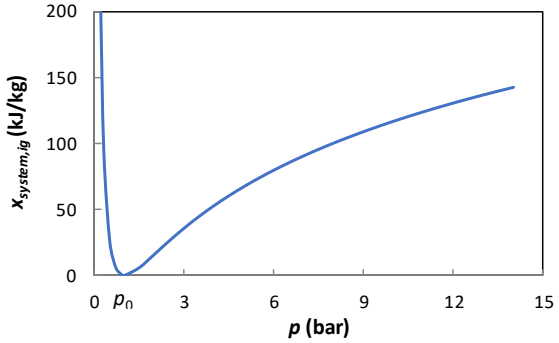

Fig. 3 Internal exergy of air as an ideal gas versus pressure at constant temperature T_0

Internal exergy of an ideal gas as a function of temperature can be obtained by substituting constant pressure p_0 in Eq. (32). The result is expressed by the following equation and shown in Fig. 4 for air.

$$X_{system,ig}(T, p_0) = m\,c_v\,T_0\left(\frac{T}{T_0} - 1 - \frac{c_p}{c_v}\ln\frac{T}{T_0}\right) + R_g\,m\,(T - T_0) \tag{34}$$

Again, there is an asymptote for $T \rightarrow 0$ and no internal exergy at T_0. At high temperatures, the linear term dominates over the logarithmic term and a linear dependency is observed. Comparing Fig. 3 and Fig. 4, it is evident that temperature has a greater impact on internal exergy than pressure.

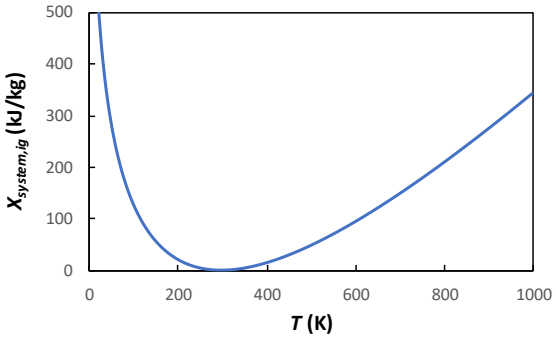

Fig. 4 Internal exergy of air as an ideal gas versus temperature at constant pressure p_0

Internal exergy of incompressible media:

Similar to the ideal gas case, internal exergy of incompressible media can be derived using the characteristic relations $u = u_0 + c(T\text{-}T_0)$, $s = s_0 + c\ln(T/T_0)$, and V = constant. Substituting these equations into Eq. (28) yields:

$$X_{system,im} = m\left[c\,(T - T_0) - T_0\,c\,\ln\frac{T}{T_0}\right] \tag{35}$$

where $X_{system,im}$ is the internal exergy of an incompressible medium. It is noted in this equation that the internal exergy of incompressible media depends only on temperature. Figure 5 shows the internal exergy of water as an incompressible material versus temperature, where, like the ideal gas case, an asymptote is observed for $T \rightarrow 0$, and no exergy at $T = T_0$. At high temperatures ($T >> T_0$) the linear term dominates over the logarithmic term and a linear dependency prevails.

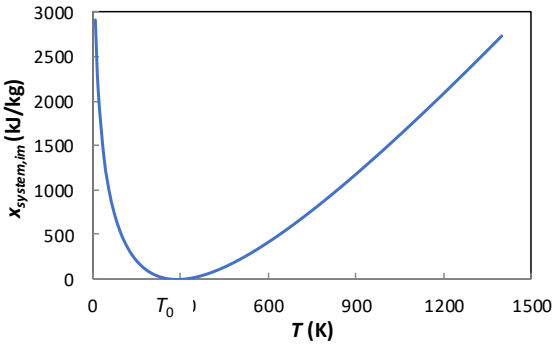

Fig. 5 Internal exergy of water as an incompressible medium versus temperature

2.2 Flow Exergy

For a stationary rigid control volume at steady-state that exchanges heat only with the environment (Fig. 6), and neglecting the kinetic and potential energy variations, Eq. (19) simplifies to:

$$\dot{W} = \sum \dot{m}_{j,in}\,(h^a - h_0^a)_{j,in} - \sum \dot{m}_{j,out}\,(h^a - h_0^a)_{j,out} - T_0\,\dot{S}_{gen} \tag{36}$$

Global Digital Central
ISSN: 2151-8629

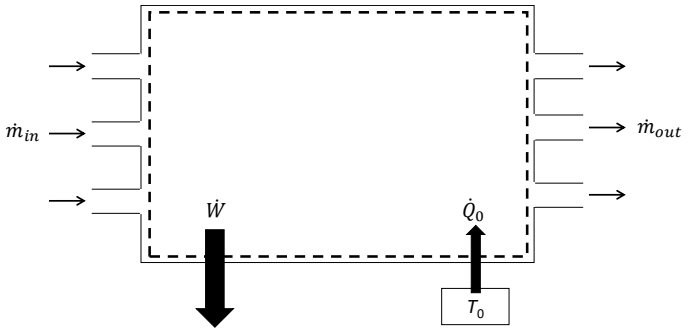

Fig. 6 Stationary and rigid control volume with negligible kinetic and potential energy exchanging heat only with the environment

If no chemical reaction takes place within the control volume, the inlet mass flow rate of each component is equal to its outlet mass flow rate and the exergy balance equation can be written as:

$$\dot{W} = \sum \dot{m}_j (\psi_{in} - \psi_{out})_j - \dot{X}_{des} \tag{37}$$

Finally, if the exiting flows are at the dead state ($\psi_{out} = 0$):

$$\dot{W} = \sum \dot{m}_j \, \psi_{j,in} - \dot{X}_{des} \tag{38}$$

For a reversible process $\dot{X}_{des} = 0$, hence:

$$\dot{W}_{rev} = \sum \dot{m}_j \, \psi_{j,in} = \sum \dot{m}_j \left[(h_{j,in} - h_{j,0}) - T_0 \, (s_{j,in} - s_{j,0}) \right] \tag{39}$$

Equation (39) shows that the property previously defined as "flow exergy" represents the reversible work obtainable from the mass flow rate of a specific component in a certain state when brought to equilibrium with the dead state.

Flow exergy of ideal gases:

The ideal gas relations $h = h_0 + c_p(T\text{-}T_0)$ and Eq. (30) can be applied to Eq. (39) to obtain the following expression for flow exergy of ideal gases:

$$\psi_{ig} = c_p \, T_0 \left(\frac{T}{T_0} - 1 - \ln \frac{T}{T_0} \right) + R_g \, T_0 \, \ln \frac{p}{p_0} \tag{40}$$

where ψ_{ig} is the flow exergy of an ideal gas. It is interesting to examine the contribution of temperature and pressure to flow exergy by alternatively fixing each at the environmental values, and plotting ψ as a function of the other variable. Doing so, the dependency of flow exergy on pressure for an ideal gas at environment temperature is described by the following equation and shown in Fig. 7:

$$\psi_{ig}(T_0, p) = R_g \, T_0 \, \ln \frac{p}{p_0} \tag{41}$$

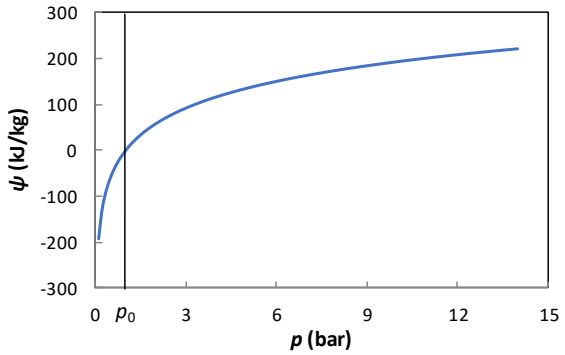

Fig. 7 Flow exergy of air as an ideal gas versus pressure at constant temperature T_0

The dependency is purely logarithmic, with an asymptote as $p \rightarrow 0$. For $p = p_0$ (dead state) the pressure contribution to flow exergy is zero. For pressure values below p_0, the flow exergy is negative. A negative exergy implies that the flow not only cannot produce work, but also the environment must do work on the flow to bring it to dead state. As the pressure increases, its effect on ψ becomes less significant. The flow exergy as a function of temperature only is described by the following equation and shown in Fig. 8:

$$\psi_{ig}(T, p_0) = c_p \, T_0 \left(\frac{T}{T_0} - 1 - \ln \frac{T}{T_0} \right) \tag{42}$$

Flow exergy is zero at the dead state ($T = T_0$), and there is no region of negative values. Again, there is an asymptote for $T \rightarrow 0$, and a linear dependency at higher temperatures. Similar to the internal exergy, it is observed that compared to pressure, the temperature has a greater effect on flow exergy of ideal gasses.

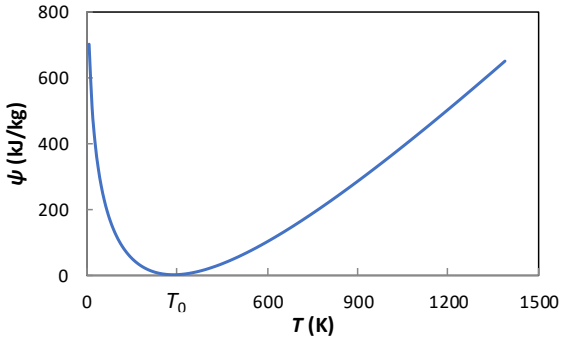

Fig. 8 Flow exergy of air as an ideal gas versus temperature at constant pressure p_0

Being able to use the ideal gas equations is particularly interesting in the case of a heat exchanger with negligible pressure drop and heat loss. This is examined by considering the system shown in Fig. 9, where the hot (cold) gas stream enters the control volume at a temperature of $T_{h,in}$ ($T_{c,in}$) and leaves the system with a temperature of $T_{h,out}$ ($T_{c,out}$).

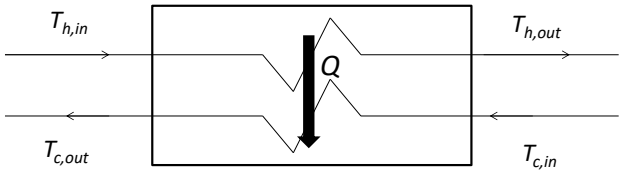

Fig. 9 Representative heat exchanger with negligible pressure drop and heat loss transferring heat between ideal gas streams

From the definition of flow exergy and the ideal gas relations, and assuming negligible pressure drop, the following exergy balance can be written for the hot fluid:

$$\begin{aligned} \Delta\psi_h &= \Delta h - T_0 \, \Delta s = c_p \left(T_{h,in} - T_{h,out} \right) - T_0 \, c_p \, \ln \frac{T_{h,in}}{T_{h,out}} \\ &= c_p \left(T_{h,in} - T_{h,out} \right) \left[1 - T_0 / \frac{T_{h,in} - T_{h,out}}{\ln (T_{h,in}/T_{h,out})} \right] \end{aligned} \tag{43}$$

Introducing the log mean temperature difference, $T_{lm} = (T_1 - T_2)/\left(\ln \frac{T_1}{T_2}\right)$, and heat transfer rper unit mass of the hot gas stream, $q = \Delta h = c_p \left(T_{h,in} - T_{h,out} \right)$, the exergy reduction of the hot stream can be expressed by:

$$\Delta\psi_h = \psi_{h,in} - \psi_{h,out} = q \left(1 - \frac{T_0}{T_{lm,h}} \right) = q \, \vartheta_{lm,h} \tag{44}$$

Global Digital Central
ISSN: 2151-8629

A similar expression can be obtained for the cold stream. These equations suggest that in a heat exchanger with two ideal gas streams and negligible pressure drop, the exergy fluxes can be viewed as the exergy flux between two reservoirs at constant temperatures, equal to the log mean temperatures of the hot and cold flows through the heat exchanger.

Flow exergy for incompressible media:

Again, the incompressible media equations $h = h_0 + c(T\text{-}T_0) + v(p\text{-}p_0)$ and $s = s_0 + c\ln(T/T_0)$ can be applied to obtain the following expression for the flow exergy of incompressible media:

$$\psi_{im} = c\,(T - T_0) + v\,(p - p_0) - T_0\,c\ln\frac{T}{T_0} \tag{45}$$

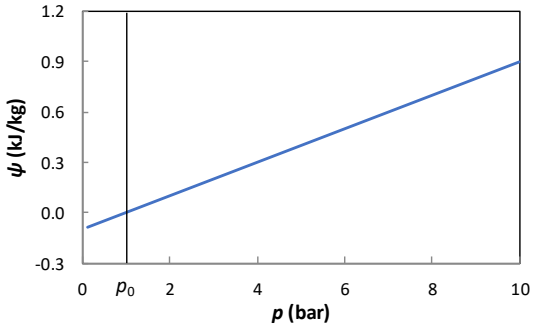

Fig. 10 Flow exergy of water as an incompressible medium versus pressure at constant temperature T_0

At a constant temperature T_0 the flow exergy of a incompressible material is simplified to $\psi_{im} = v\,(p\text{-}p_0)$. The linear variations of the flow exergy of an incompressible medium (water) with pressure at constant temperature T_0 are shown in Fig. 10. It should be noted in Fig. 10 that pressure has only minor effects on flow exergy. For $p < p_0$, the flow exergy is negative which means for the flow to come to equilibrium with the environment, a net amount of work must be done on the flow by the environment.

Temperature dependence of the flow exergy of an incompressible medium at constant pressure ($p = p_0$) is described by:

$$\psi_{im}(T, p_0) = c\,T_0\left[\frac{T}{T_0} - 1 - \ln\frac{T}{T_0}\right] \tag{46}$$

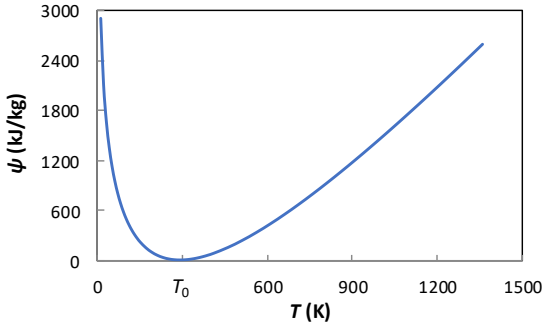

Fig. 11 Flow exergy of water as an incompressible medium versus temperature at constant pressure p_0

Figure 11 shows the variations of flow exergy of water as an incompressible medium versus temperature at a constant pressure p_0. As evident, the effect of temperature on the flow exergy is much greater compared to pressure. Hence, it can be concluded that the temperature is the dominant factor in flow exergy of an incompressible medium.

2.3 Thermal Exergy

As shown before, thermal exergy represents the amount of work that can be obtained by exploiting the amount of heat available at a certain temperature through a reversible Carnot engine:

$$\dot{W}_{rev} = \dot{Q}\,\eta_{carnot} = \dot{Q}\left(1 - \frac{T_0}{T}\right) = \dot{X}_{heat} \tag{47}$$

2.4 Chemical Exergy

In the analyses presented so far, the presence of chemical reactions in the systems has been neglected. However, several systems used for power generation involve combustion processes. In order to properly characterize these systems, the maximum amount of work that could be obtained by full utilization of the chemical energy should be determined.

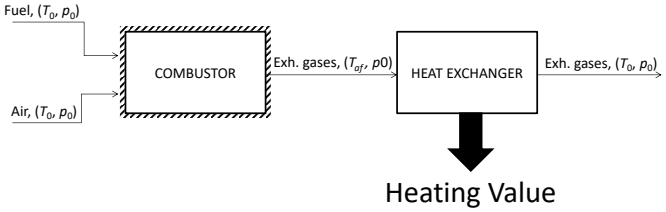

Fig. 12 Schematic representation of traditional way of heating value measurement

In the traditional approach, this objective is achieved by measuring the *heating value* (HV), or *heat of combustion*, characterizing the combustible. The HV represents the amount of heat generated by a complete stoichiometric combustion of a unitary quantity of the combustible. A diagram of the measurement technique can be seen in Fig. 12. Both the combustible and air enter the adiabatic combustion chamber at p_0 and T_0; once the combustion occurs and the combustible is completely oxidized, the exhaust gases will be at a specific temperature, called the *adiabatic flame temperature* (T_{af} in Fig. 12). The heat of combustion is the thermal energy released as the exhaust gases are brought back to the reference conditions, T_0 and p_0.

The heat of combustion, however, does not correspond exactly to the maximum work that can be obtained from this process. In order to find the maximum work potential of a combustion process, the process of thermal energy conversion needs to be investigated in more detail. This is done by considering the control volume in Fig. 13 in which all reagents enter and exit the system at T_0 and p_0 while heat exchange is allowed only with the environment and work is done by the system.

The energy and entropy balances for the control volume of Fig. 13 should include the formation entropy and enthalpy for both reactants and products to account for the chemical reactions that occur inside the system. The energy balance for the control volume per unit mass is:

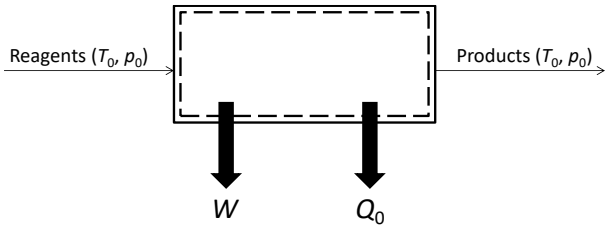

Fig. 13 Control volume employed for the analysis of ideal reaction

$$\sum h^f_{R,j}(T_0, p_0) = \sum h^f_{P,j}(T_0, p_0) + q_0 + w \tag{48}$$

where $h^f_{R,j}$ and $h^f_{P,j}$ denote the specific enthalpy of formation of the j^{th} component of reactants and products and w and q_0 are the specific work and heat transfer, respectively.

The entropy balance for the control volume can be written as:

$$\frac{q_0}{T_0} + \sum s^f_{P,j}(T_0, p_0) - \sum s^f_{R,j}(T_0, p_0) = s_{gen} \tag{49}$$

DOI: 10.5098/hmt.12.9 ISSN: 2151-8629

where $s^f_{R,j}$ and $s^f_{P,j}$ are the specific entropy of formation of the j^{th} component of reactants and products, respectively.

Multiplying Eq. (49) by T_0 and combinging with Eq. (48) yields:

$$w = \left[\sum h^f_{R,j}(T_0,p_0) - \sum h^f_{P,j}(T_0,p_0)\right] - T_0\left[\sum s^f_{R,j}(T_0,p_0) - \sum s^f_{P,j}(T_0,p_0)\right] - T_0\, s_{gen} \quad (50)$$

The maximum amount of work, w_{rev}, is obtained in a reversible process when $s_{gen} = 0$. Recalling the definition of Gibbs free energy, $g = h - Ts$, the reversible work can be expressed as:

$$w_{rev} = \sum g^f_{R,j}(T_0,p_0) - \sum g^f_{P,j}(T_0,p_0) = -\Delta g^f_{Comb}(T_0,p_0) \quad (51)$$

where $g^f_{R,j}$ and $g^f_{P,j}$ are the specific Gibbs free energy of formation of the j^{th} component of reactants and products, respectively.

Typically, the values of Δg and HV are close to each other, meaning that the maximum work obtainable with reversible combustion of fuel is not far from the heat released during combustion. However, the combustion process involves a degradation in the availability of chemical energy, limiting the potential conversion because of the finite adiabatic flame temperature. In other words, it is not possible to achieve a full conversion of heat to work, unless the adiabatic flame temperature goes to infinity.

A small correction has to be made in order to complete the definition of chemical exergy. In an ideal system (Fig. 13) it was assumed that both reactants and products are in the dead state. For the fuel this may be true, but the pressure of the oxygen in the environment is not p_0, but at its partial pressure, equal to its molar fraction times p_0. In order to bring the oxygen pressure to the hypothesized entering conditions, an imaginary process of isothermal compression preceding the reaction chamber should be considered that will require a certain amount of work (Eq. 41). Similarly, the partial pressures of the products will be different from their partial pressures in the environment; this would theoretically allow for running a turbine to exploit this pressure difference as the products expand to their environmental partial pressure. As such, a precise definition of the chemical composition of the dead state becomes essential when dealing with chemical exergy.

Considering the total contributions from the compression/expansion just described, an expression for the chemical exergy of a combustible can be derived. By adopting an ideal gas assumption:

$$w_{rev} = -\Delta g^f_{Comb}(T_0,p_0) + \left(\sum_P w_{turb} - \sum_R w_{compr}\right) = -\Delta g^f_{Comb}(T_0,p_0) + \sum_j N_j\, R\, T_0 \ln\frac{p_j}{p_{0,j}} = x_{ch} \quad (52)$$

where N_j is the number of moles of the j^{th} component, $p_{0,j}$ is its partial pressure in the dead state, and x_{ch} is defined as the *chemical exergy* of the substance. Values for this property can be found in thermodynamic tables. This helps to achieve a better understanding of the process of combustion and the losses it generates in energy systems. Comparison between the total exergy (chemical, flow, etc.) of the reactants and products of a combustion process shows that the *exergy efficiency* of a combustion process is far below 100% (usually around 60-70%).

2.5 Exergy Destruction

From the second law, the total entropy of an isolated system has to remain constant or increase due to the irreversibilities taking place inside the system. Increase of entropy is represented by the term $\dot{S}_{gen}$ in the entropy balance equation, Eq. (8), which is either zero when the process is reversible or positive when it is not. It can be seen in Eq. (23) that the product $T_0\dot{S}_{gen}$ represents the difference between the reversible work and the actual work. As noted earlier, $\dot{S}_{gen}$ never possesses negative values, thus, reversible work delivery will always be greater than actual work delivered. As such, $T_0\dot{S}_{gen}$ (or equivalently $\dot{X}_{des}$) represents a loss in the work potential of any system $\left(\dot{X}_{des} = T_0\dot{S}_{gen} > 0\right)$. Exergy is thus not conserved but is constantly decreasing due to the entropy generation by irreversible processes; this is also known as the decrease of exergy principle.

3. EXERGY EFFICIENCY

In the previous sections it was established how the concept of exergy facilitates a direct comparison between different forms of energy at different levels of thermodynamic quality. For example, for a certain amount of mechanical energy, there is a corresponding amount of heat, depending on the temperature at which this heat is available. A new efficiency parameter, namely the *exergy efficiency* or *second law efficiency*, accounts for the difference in the exergy content of the energy fluxes entering and leaving the system:

$$\eta_{II} = \frac{\text{Exergy output}}{\text{Exergy input}} \quad (53)$$

Using the exergy balance, the above equation can be rewritten as:

$$\eta_{II} = \frac{\text{Exergy input} - \text{Destroyed exergy}}{\text{Exergy input}} = 1 - \frac{X_{des}}{X_{in}} \quad (54)$$

This equation shows how a process in which there is exergy destruction (or equivalently entropy generation) is a direct cause of performance loss. Considering an electric heater, while the exergy input is equal to the electric energy consumption (electrical energy is equivalent to work), the exergy of output heat is much less due to the Carnot factor ($1 - T_0/T_h$), even though the output heat has the same amount of energy as the input electricity. Consequently, the second law efficiency of this energy conversion process is far from unity and much closer to zero (depending on the actual log mean temperature of the hot air produced).

In the case of devices that consume heat at specific temperature T_h to produce work, the general definition of the second law efficiency can be written as:

$$\eta_{II} = \frac{X_{out}}{X_{in}} = \frac{W_u}{Q_{in}\,\vartheta_{in}} = \frac{\frac{W_u}{Q_{in}}}{1 - \frac{T_0}{T_h}} = \frac{\eta_{th}}{\eta_{th,Carnot}} \quad (55)$$

where W_u is the actual work produced and η_{th} is the actual energy efficiency ($\eta_{th} = W_u / Q_{in}$). The second law efficiency is equal to the ratio of the actual energy efficiency of the engine to the maximum theoretical efficiency of an engine operating between T_h and T_0 (the Carnot efficiency). The exergy efficiency can be used for general characterization of the thermodynamic quality of a device, showing how far from the maximum achievable performance it is operating, and allowing for comparison between different engines or cycles with different maximum temperatures.

The efficiency of work-consuming devices that have a useful thermal effect can be defined as:

$$\eta_{II} = \frac{X_{out}}{X_{in}} = \frac{Q_u\,\vartheta_u}{W_{in}} = \frac{\frac{Q_u}{W_{in}}}{\left|\left(1 - \frac{T_0}{T_u}\right)\right|^{-1}} = \frac{\text{COP}}{\text{COP}_{rev}} \quad (56)$$

where Q_u is the actual desired thermal effect (heating or cooling) delivered at temperature T_u ($T_u > T_0$ for heating and $T_u < T_0$ for cooling), and COP is the coefficient of performance of the device ($\text{COP} = Q_u / W_{in}$). For the work-producing devices, the second law efficiency is the ratio between the actual performance and the ideal performance in the same

Global Digital Central
ISSN: 2151-8629

conditions. It is thus independent from the conditions themselves and can be used to compare different devices operating in different circumstances.

The second law efficiency is always smaller than 100% due to irreversibilities and thermodynamic limits of performance. It is impossible to construct a device that has a higher efficiency than a reversible machine. At its best, a thermodynamic system will be able to achieve the same performance as its reversible counterpart, yielding a second law efficiency of 100%.

Considering a thermodynamic system that is comprised of *n* components, the total exergy destruction can be divided into *n* different sub-destructions associated with each component. This will allow for the description of every component of the system in terms of global inefficiency, and show where the largest margins for improvements lie:

$$X_{des} = \sum_j X_{des,j} \tag{57}$$

$$\eta_{II} = 1 - \frac{X_{des}}{X_{in}} = 1 - \frac{\sum_j X_{des,j}}{X_{in}} \tag{58}$$

Being able to identify the causes of irreversibility does not always lead to efficiency improvement. For instance, in turbo-gas engines the combustion process is a major cause for the loss in performance. However, unless the combustion is substituted with an oxidation process that does not pass through the generation of heat, the only way of limiting this irreversibility is increasing the temperature at which the combustion takes place. In this way, the heat will be available at a higher temperature, and the loss in thermodynamic quality of energy will be reduced.

4. CASE STUDIES

In this section, application of the exergy analysis to representative engineering systems is demonstrated. Examples include direct methanol fuel cells, solar thermal energy storage systems, heat exchangers and thermal desalination.

4.1 Second Law Analysis of Fuel Cell Systems

Fuel cells are electrochemical energy devices that convert chemical energy of a fuel into electricity through a chemical reaction with an oxidizer. Unlike conventional power cycles such as Rankine, Brayton, or Otto cycles, the first law performance of fuel cells is not limited by the Carnot efficiency, allowing them to achieve theoretical efficiencies as high as 90%. The major types of fuel cells include the alkaline fuel cell (AFC), proton exchange membrane fuel cell (PEMFC), direct methanol fuel cell (DMFC), molten carbonate fuel cell (MCFC), phosphoric acid fuel cell (PAFC), and solid oxide fuel cell (SOFC). Among these fuel cell types, DMFCs are of great interest to provide power to many portable, low-temperature applications such as laptops and cell phones.

Major components of a fuel cell include the anode diffusion layer, anode catalyst layer, ion conducting electrolyte (membrane), cathode catalyst layer, and cathode diffusion layer. On the anode side, the fuel passes through a diffusion layer to the hydrated catalyst layer where it breaks down into electrons and protons. The protons diffuse through the electrolyte membrane and reach the cathode catalyst layer, while the electrons flow to the cathode side through an external circuit, generating electrical current. In the cathode catalyst layer, the oxidizing agent, protons, and electrons react and produce water. The anode and cathode side reactions in a DMFC are, respectively:

$$CH_3OH + H_2O \rightarrow CO_2 + 6H^+ + 6e^- \tag{59}$$

$$\frac{3}{2}O_2 + 6H^+ + 6e^- \rightarrow 3H_2O \tag{60}$$

Direct methanol fuel cells are categorized as a low-temperature fuel cells with a proton conductive polymer electrolyte membrane. They offer the advantage of simple structure and instantaneous charging time in comparison to lithium-ion batteries. However, there are still some barriers hindering commercialization of DMFCs, including water and methanol crossover through the membrane, and slow methanol oxidation kinetics at the anode. Exergy analysis is a useful tool that identifies exergy flow in and out, as well as exergy destruction sources within the fuel cell, thereby enabling an improved design of DMFCs.

There are several sources of irreversibility in the operation of a fuel cell, including overpotentials at the anode and cathode sides, crossover of the fuel through the membrane, limited proton conductivity of the membrane, and contact resistances. It is noted that overpotentials are losses associated with the kinetics of the electrochemical reaction taking place in the catalyst layer. Bahrami and Faghri (2011) developed an analytical, one-dimensional, steady-state model to predict the contribution of each of the exergy destruction sources on the overall second law performance of a passive DMFC. The effect of methanol concentration on various exergy destruction sources was also studied.

Figure 14 shows the details of the exergy destruction and the contribution of each irreversibility source, where the term "Other" refers to the exergy loss due to phase change, mixing of the components in the system, and friction. As shown in Fig. 14, the exergy losses due to the anode and cathode overpotentials are very significant at higher cell current densities. While the exergy loss due to methanol crossover decreases monotonically as the cell current density increases for the case of 1 M methanol concentrations (1 mole of methanol in 1 L of the fuel solution) in the fuel tank, an initial increase followed by a final reduction is observed when 3 M methanol concentration is present at the anode.

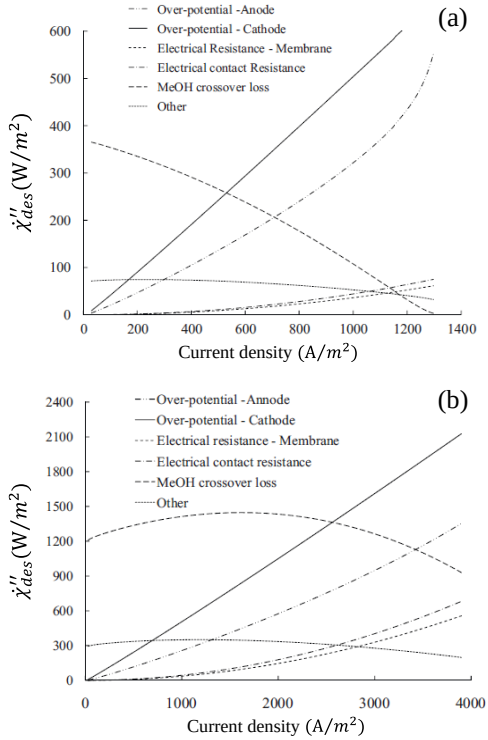

Fig. 14 Different irreversibilities present in a DMFC versus cell current density for fuel methanol concentrations (a) 1 M, and (b) 3 M

It was also found that the exergy efficiency of a passive DMFC decreases as the concentration of the methanol solution in the tank increased, as opposed to the first law efficiency which increases with increased methanol concentration of the fuel.

The overall exergy analysis yields only aggregate values for the overall exergy losses in fuel cells. However, to optimize the cell structure or the properties of various cell components, the overall exergy analysis does not provide enough detailed information. In this case, the local entropy generation analysis method should be used to determine the location and individual contributions of identified exergy losses within the fuel cell. To this end, Li and Faghri (2011) conducted a local entropy

generation analysis based on a two-dimensional, two-phase, non-isothermal DMFC model, where the entropy generation due to chemical reactions, heat transfer, mass diffusion, and viscous dissipation were investigated. The continuity, momentum, energy, and species equations were solved with the inclusion of local entropy generation along with the overall exergy balance equations.

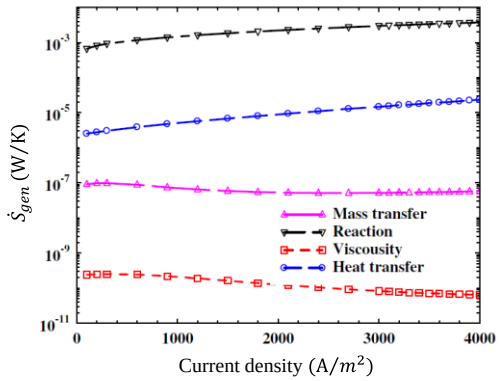

Fig. 15 Mechanisms of entropy generation in a passive DMFC (3 mm MBL; 125 mm PEM; room temperature; 16 M methanol)

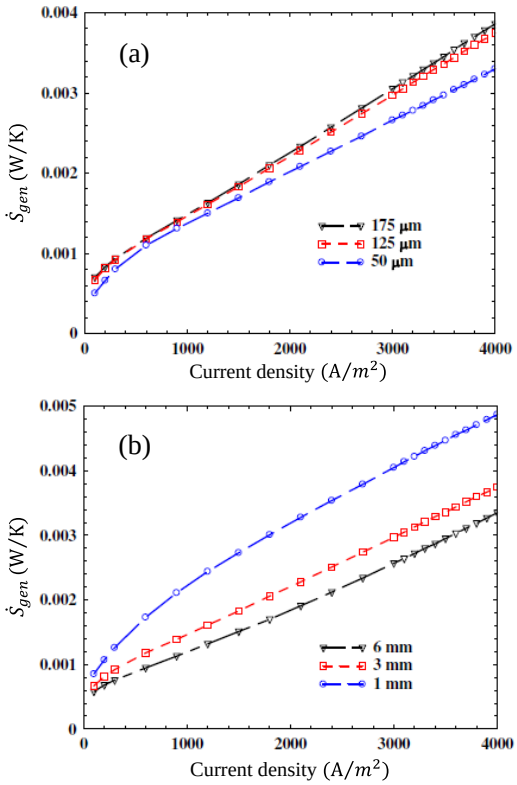

Fig. 16 Entropy generation rates within a passive DMFC for (a) various electrolyte membrane thicknesses, and (b) various MBL thicknesses

Figure 15 shows the entropy generation rates due to heat transfer, mass transfer, viscous dissipation, and chemical reactions. It is evident from this figure that entropy is mainly generated by the consumption of fuel through the electrochemical reactions. The irreversible heat transfer driven by temperature gradients within the cell is the second largest entropy generation source and is about two orders of magnitude smaller than the reaction-related losses. The entropy generation due to both viscous dissipation and mass diffusion (driven by the species gradients within the fuel cell) is relatively small compared with that from the chemical reaction and heat transfer.

The local entropy generation rates were used for structural optimization of a passive DMFC. To do so, the effect of the thickness of the membrane and the methanol barrier layer (a layer positioned between the fuel reservoir and anode diffusion layer intended to control the flow of methanol solution into the cell) on the overall entropy generation rate of the DMFC were investigated. As shown in Fig. 16, the overall entropy generation decreases with a decreasing membrane thickness or with an increasing methanol barrier layer thickness.

4.2 Exergy Analysis of Latent Heat Thermal Energy Storage for Concentrating Solar Power Application

Thermal energy storage is the key to large-scale deployment of concentrating solar power (CSP) generation. Among various storage technologies, latent heat thermal energy storage (LHTES) is attractive due to large energy storage densities and virtually isothermal behavior. In LHTES systems, a portion of the absorbed solar thermal energy is transferred to the LHTES system via a heat transfer fluid (HTF) and is stored mainly in the form of the latent heat of fusion of a phase change material (PCM). The thermal energy is released at times of demand as the molten PCM solidifies. There are several heat transfer processes involved in the charging-discharging operation of a LHTES system, with the exergy destruction accompanying the heat transfer identified as the major source of irreversibility (Shabgard *et al.*, 2018). The greater the temperature difference between the HTF and PCM, the greater the rates of exergy destruction. A PCM with a relatively low melting temperature leads to relatively large temperature differences between the HTF and PCM during charging, therefore increasing the exergy destruction rates. Conversely, a PCM with relatively high melting temperature results in increased exergy destruction rates during discharge due to greater temperature differences between the PCM and HTF. This brings about a dilemma in selection of a PCM for operation in charging-discharging cycles.

Several investigators have carried out exergy analysis of LHTES systems during charging or discharging modes of operation. However, since the operation of LHTES systems involves multiple charging-discharging cycles, the exergy analysis is most useful when cyclic operation is considered. A common approach to reduce the irreversibility in LHTES systems is using multiple PCMs with decreasing melting temperatures in the direction of the HTF flow during charging (PCM melting). The HTF flow is reversed during discharge to keep the local temperature differences within the system more uniform. Shabgard *et al.* (2012) developed a thermal network model to study the exergy efficiency of cascaded and non-cascaded heat pipe-assisted LHTESs during a charging-discharging cycle. The exergy efficiency was defined as the ratio of the exergy increase of the HTF during the discharge process to the total exergy content of the HTF at the inlet of the LHTES during charging. This definition of exergy efficiency takes into account the effectiveness of the LHTES in absorbing (releasing) thermal energy from the HTF during charging (discharging) and returns a value of zero when there is no heat transfer between the PCM and the HTF. For any charging duration, the discharge process continued until the entire thermal energy stored during charging was recovered.

Figure 17 shows the exergy efficiency of charging-discharging cycles with various charging durations for cascaded and non-cascaded LHTESs. The maximum charging time for each system corresponds to an overall charging–discharging cycle duration of 24 h. In all cases, the exergy content of the HTF leaving the LHTES during charging is considered as lost. In addition, there are exergy losses due to the temperature differences accompanying heat transfer during both charging and discharging. The exergy loss associated with the HTF leaving the LHTES during charging is the biggest contributor to the relatively low exergy efficiency of the systems considered here. Also, as evident, the LHTES with the smallest melting temperature (318 °C) provides the highest exergy efficiency, however, it also corresponds to the shortest maximum possible charging time. Hence, it may not be the appropriate choice depending on the time available for charging.

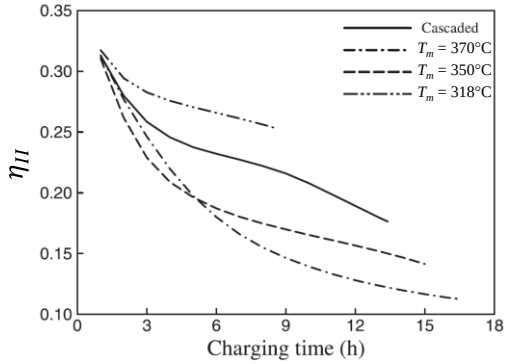

Fig. 17 Exergy efficiency of a charging-discharging cycle for various LHTES systems with various charging times

The duration of the charging-discharging cycles of the thermal energy storage system in solar applications is limited to 24 h. As such, the optimal design of a LHTES must comply with this limited charging and discharging time. The time constraint has not been accounted for in most heat transfer or exergy analyses of the LHTES systems available in literature. As a result, in some cases optimum LHTES performance corresponds to infinite discharging times, limiting the practical usefulness of the analyses.

Shabgard *et al.* (2013) performed a combined heat transfer and exergy analysis of a LHTES system for CSP to investigate the optimal design accounting for the finite duration of a charging-discharging cycle. Two practical constraints, namely (*i*) the equality of the energy stored and recovered, and (*ii*) the finite duration of the charging-discharging cycle imposed by the solar day were considered. Similar to Shabgard *et al.* (2012), exergy efficiency was defined as the ratio of the exergy recovered by the HTF during the discharge to the total exergy content of the HTF at the inlet of the LHTES during charging. It was found that the maximum exergy efficiency corresponds to infinitely small thermal energy storage. Because of the limited practical utility of exergy efficiency, maximizing the exergy recovery was selected as the objective of the optimization.

For any specific value of the HTF inlet temperature during charging, specific values of HTF inlet temperature during discharge and PCM melting temperature are required to maximize either the thermal energy stored/recovered, or the exergy recovered. The predicted values for optimal melting temperature and discharge HTF inlet temperature corresponding to maximum energy storage/recovery, η_{max}, or the maximum exergy recovery, χ_{max}, are presented in Fig. 18. It is noted that in this figure the temperatures are presented in non-dimensional form, $\bar{T} = T/T_0$, where T_0 is the ambient temperature. The dimensionless temperature $\bar{T}_{m,max}$ is the phase change temperature required to maximize either the energy stored or the exergy recovered. It is shown in

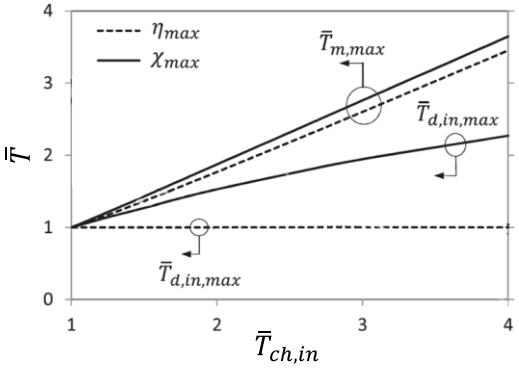

Fig. 18 PCM melting temperatures and discharge HTF inlet temperatures corresponding to the maximum energy storage and exergy recovery for various charging HTF inlet temperatures

Fig. 18 that $\bar{T}_{m,max}$ increases as the HTF inlet temperature during charging, $\bar{T}_{ch,in}$, increases. Similarly, the required HTF inlet temperature during discharging, $\bar{T}_{d,in,max}$, should be increased with increasing $\bar{T}_{ch,in}$ if the objective is to maximize the recovered exergy. On the other hand, $\bar{T}_{d,in,max}$ should be set to 1 to achieve the maximum energy storage. Because of the dependence of the extracted exergy on the HTF outlet temperature, the required phase change temperature to maximize exergy recovery always exceeds that necessary to maximize energy storage.

The developed model was applied to ascertain the performance of several practical CSP technologies. A quantitative result obtained from this study was that for a typical salt PCM, the optimal phase change temperatures corresponding to charging HTF inlet temperatures of 560 °C and 800 °C were found to be 475 °C and 715 °C, respectively. The second law performance of the storage system can be improved, and the potentially impractical optimal operating conditions can be avoided by modifying the heat transfer design of the energy storage system. For example, it was found that by a 10 times increase in the surface area of the PCM side of the LHTES system, a six-fold increase in the exergy extracted from the LHTES system can be achieved.

4.3 Second Law Analysis of Heat Exchangers

Energy waste in any form results in a decrease of available work potential. The losses of useful work due to process irreversibilities can be calculated using the concept of entropy generation minimization. The entropy generation minimization approach was first used for the analysis of heat exchangers in the 1950s, and the irreversibility concept was first employed for heat exchanger design in 1951 by McClintock (1951). There are three basic types of exergy losses that occur in a typical heat exchanger, (*i*) losses due to the exchange of heat across a finite temperature difference, (*ii*) losses due to fluid friction, and (*iii*) losses due to heat exchange with the environment. The losses to the environment are usually relatively small because the heat exchanger surface is normally insulated to reduce such an exchange of heat. There exists a direct proportionally between the irreversibility (quantified as the entropy generated) and the amount of available work lost in the process. Second law analysis seeks to minimize these losses by keeping entropy generation to a minimum.

For a balanced counterflow heat exchanger ($\dot{m}_c c_{p,c} = \dot{m}_h c_{p,h}$), the entropy generation rate due to heat transfer between the hot and cold media is:

$$\dot{S}_{gen} = \dot{m} c_p \ln \left[\frac{\left(1 + \frac{T_{c,in}}{T_{h,in}} NTU\right)\left(1 + \frac{T_{h,in}}{T_{c,in}} NTU\right)}{(1 + NTU)^2} \right] \tag{61}$$

The entropy generation rate is generally expressed in a dimensionless form. The most obvious way of non-dimensionalizing entropy generation rate is to divide it by the heat capacity rate $\dot{m} c_p$:

$$N_s = \frac{\dot{S}_{gen}}{\dot{m} c_p} = \ln \left[\frac{\left(1 + \frac{T_{c,in}}{T_{h,in}} NTU\right)\left(1 + \frac{T_{h,in}}{T_{c,in}} NTU\right)}{(1 + NTU)^2} \right] \tag{62}$$

The dimensionless entropy generation number may also be presented in terms of heat exchanger effectiveness, ε:

$$N_s = \frac{\dot{S}_{gen}}{\dot{m} c_p} = \ln \left[\left(1 + \varepsilon \left(\frac{T_{h,in}}{T_{c,in}} - 1 \right) \right) \left(1 - \varepsilon \left(1 - \frac{T_{c,in}}{T_{h,in}}\right)\right) \right] \tag{63}$$

This function is illustrated in Fig. 19. As noted by Bejan (1996), N_s approaches zero in two limits: $NTU \to \infty$ ($\varepsilon \to 1$) and $NTU \to 0$ ($\varepsilon \to 0$). Bejan calls this behavior the "entropy generation paradox" and the $NTU \to 0$ limit the "vanishing heat exchanger limit".

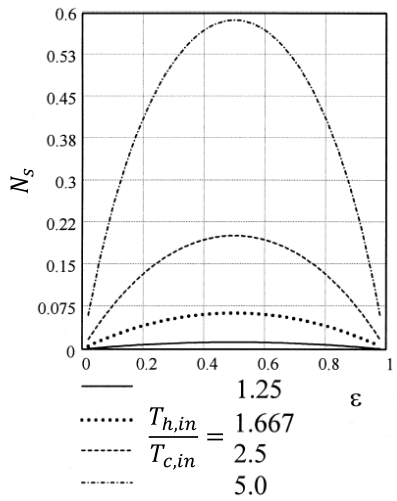

Fig. 19 Variations of the entropy generation number with heat exchanger effectiveness

Hesselgreaves (2000) suggested dividing the entropy generation rate by $\dot{Q}/T_{c,in}$, where $\dot{Q}$ is the heat transfer rate of the heat exchanger, to eliminate Bejan's paradox. Using this description, the new entropy generation number, $N_{s,1}$ for a balanced counterflow heat exchanger is:

$$N_{s,1} = \frac{T_{c,in}\,\dot{S}_{gen}}{\dot{Q}} = \frac{N_s}{\varepsilon\left(\frac{T_{h,in}}{T_{c,in}} - 1\right)} \tag{64}$$

Figure 20 shows the modified entropy generation number versus heat exchanger effectiveness. As evident, the ratio $N_{s,1}$ now behaves in a more intuitive way, completing the resolution of the Bejan's paradox.

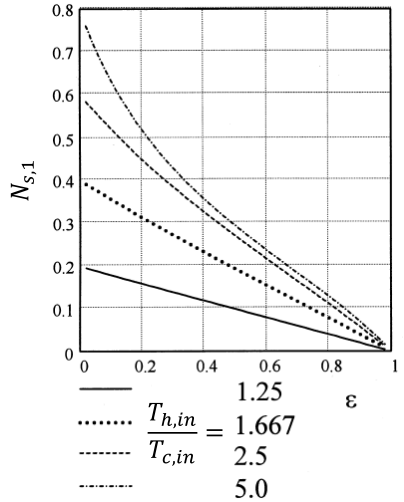

Fig. 20 Variations of the modified entropy generation number with heat exchanger effectiveness

4.4 Exergy Analysis in Thermal Desalination Systems

The performance of desalination systems should be quantified from the viewpoints of both the first and second laws of thermodynamics. In thermal desalination, the most common energy and exergy performance metrics are the gained output ratio (GOR) and the second law efficiency, respectively. The GOR is defined as either a mass ratio (mass of distilled water to the mass of steam driving the desalination process) or an energy-based GOR defined as (Mistry *et al.*, 2011):

$$\mathrm{GOR} = \frac{\dot{m}_d h_{fg}}{q} \tag{65}$$

where $\dot{m}_d$, h_{fg} and q are the production rate of distillate mass, heat of vaporization of water, and heat transfer rate to the desalination system, respectively.

The general exergy balance for a thermal desalination system operating under steady-state and with negligible work interactions can be written as:

$$\dot{X}_{th,in} + \dot{X}_f = \dot{X}_{th,out} + \dot{X}_d + \dot{X}_b + \dot{X}_{des} \tag{66}$$

where $\dot{X}_{th}$ shows the thermal exergy, $\dot{X}_f$, $\dot{X}_d$ and $\dot{X}_b$ denote the exergy flow associated with the feed, distillate and brine streams, and $\dot{E}x_{des}$ is the rate of exergy destruction, respectively. Several definitions of second law efficiency have been reported in the literature (Piacentino, 2015). One type of second law efficiency is defined as the ratio of the output exergy to the input exergy:

$$\eta_{II,1} = \frac{\dot{X}_{out}}{\dot{X}_{in}} = 1 - \frac{\dot{X}_{des}}{\dot{X}_{in}} \tag{67}$$

The total exergy destruction can be determined by adding the exergy destruction due to irreversibilities in all the system components. It is noted that in this definition, the exergy leaving the system due to the heat rejection to the ambient is not considered destroyed. This definition is more helpful when identification of the exergy destruction sources and possible remediation are of primary interest.

In another definition, the second law efficiency is defined as the ratio of the exergy of the useful product of the desalination system (i.e. the purified water) to the required exergy input. In a thermal desalination system, thermal energy supplies the required exergy input, thus, the exergy efficiency can be written as (Mistry and Lienhard V, 2013a):

$$\eta_{II,2} = \frac{\dot{X}_d}{\dot{X}_{th,in}} = \frac{\dot{X}_d}{q(1 - \frac{T_0}{T_h})} \tag{68}$$

where T_0 and T_h are the reference temperature and the temperature at which thermal energy is supplied to the system, respectively. It is noted that the efficiencies obtained from Eqs. (67) and (68) are identical if the exergy content of all the heat and flow streams leaving the desalination system, except from the distilled water, are considered as lost and the feed water is at total dead state. In the following, determination of the exergy of the distilled water is discussed.

The exergy of a multi-component flow with n constituents can be calculated from (Bejan, 2006):

$$\dot{X} = \dot{m}\left[(h - h_{RDS}) - T_0(s - s_{RDS}) + \sum_{i=1}^{n} \frac{w_i}{M_i}\left(\mu_{i,RDS} - \mu_{i,TDS}\right)\right] \tag{69}$$

where, h and s show the specific enthalpy and specific entropy and μ_i, w_i, and M_i represent the chemical potential, mass fraction and molar mass of component i in the mixture, respectively. Also, subscripts *RDS* and *TDS* refer to the restricted dead state and total dead state, respectively. At the restricted dead state, the temperature and pressure of the flow are at equilibrium with the environment while the flow composition is kept unchanged. At the total dead state, in addition to the temperature and pressure, the chemical composition of the system is also brought to equilibrium with the environment.

As noted before, atmospheric pressure and a temperature of 25°C are widely used as the restricted dead state. The definition of the chemical composition of the total dead state is not as straightforward. In seawater desalination systems, usually the seawater salinity of 35 g/kg is considered as the composition of the total dead state. For desalination systems where the input saline water is at different salinities, it is reasonable to consider the chemical composition of the available feed stream as the chemical composition of the environment. Such a choice of the total dead state composition ensures that any process which results in two streams of water with relatively higher and relatively lower

Global Digital Central
ISSN: 2151-8629

concentrations with respect to the feed water will entail an increase in the exergy of both produced streams, and hence will consume work. It is noted that the sum of the first two terms in the right-hand side of Eq. (69) represents the physical exergy and the last term shows the chemical exergy.

The easiest way to calculate the chemical exergy is by assuming the saline water as an ideal solution of sodium chloride and water. The ideal solution assumption implies that the intermolecular forces are equal between all components of the solution (Na^+- H_2O, Cl^- - H_2O, H_2O-H_2O in H_2O-NaCl solution). Therefore, there is no change of enthalpy upon replacing the bonds between some water molecules with ion-water bonds. It can be shown that for such an ideal solution, the exergy of pure water at the reference temperature and pressure (T_0 and p_0) with respect to the feed water as the total dead state is (Lienhard V *et al.*, 2017):

$$\dot{X}_{ch,d} = -\dot{m}_d \frac{R_u T_0}{M_{\mathrm{H_2O}}} \ln x_{w,f,dis} \tag{70}$$

where $x_{w,f,dis}$ is the dissociated mole fraction of the water in the saline feed water. For NaCl-water solution $x_{w,f,dis} = n_w/(n_w + 2n_s)$, where n_w and n_s show the number of moles of water and NaCl in the solution, and factor 2 in the denominator is to account for breaking of each NaCl molecule into 2 ions (dissociation). For small salinities, Eq. (70) can be further simplified by using Taylor expansion of the logarithmic term and replacing the water mole fraction with the salt mole fraction from $x_{s,f} = 1 - x_{w,f}$, to yield $\dot{X}_{ch,d} = \dot{m}_d R_u T_0 x_{s,f}/M_{\mathrm{H_2O}}$.

The amount of salt in the saline water is usually specified in terms of salinity, *S*, defined as the mass of salt dissolved in the unit mass of the solution. If the mass of salt is measured in grams and the solution mass is expressed in kilogram, the salinity is known as ppt (part per thousand). Having the salinity in ppt, the dissociated water mole fraction in Eq. (70) can be calculated as $x_{w,f,dis} = (1000 - S)/(1000 - S + 2SM_{\mathrm{H_2O}}/M_s)$. The exergy of the distilled water can be approximated by replacing Eq. (70) into Eq. (69). It is noted that more accurate expressions for the chemical exergy of water mixtures can be derived by accounting for the nonideality of the solution (Mistry and Lienhard V, 2013b).

An alternative approach to calculate the exergy of the distilled water is using the tabulated values for enthalpy, entropy and chemical potential of saline water directly in Eq. (69). Such tabulated properties have been compiled for seawater and are available for a wide range of practical temperatures, pressures and salinities (Nayar *et al.*, 2016; Sharqawy *et al.*, 2010). Available correlations in these databases allow for determination of exergy at various total dead state temperatures, pressures and salinities. For this case study, the exergy efficiencies are calculated using both the tabulated exergy values and the simplified exergy values calculated based on the ideal solution approximation in Eq. (70).

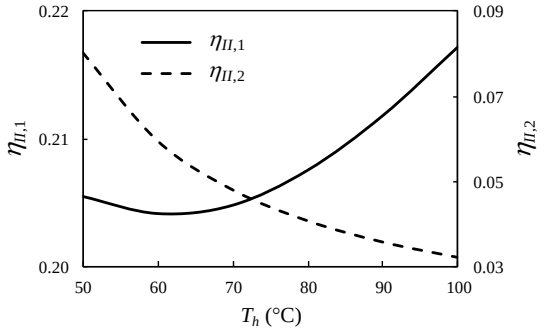

Fig. 21 The variations of the second law efficiencies with the heat source temperature

There are two types of commercial thermal desalination systems, namely the multi-stage flash (MSF) and multiple-effect distillation (MED). In both MSF and MED systems, several stages of consecutive evaporation and condensation processes occur in a decreasing pressure (and temperature) order to recover the thermal energy released by condensing vapor to drive evaporation at a lower pressure. The MED systems generally have better energy and exergy efficiencies compared to the MSF systems (Blanco *et al.*, 2009; Warsinger *et al.*, 2015). The most important factors affecting the second law efficiency of the MSF and MED systems are the number of stages, temperature at which thermal energy is supplied and quality of the input water. Figures 21 to 23 show both types of the second law efficiencies defined by Eqs. (67) and (68) for a particular MED system design. Figure 21 shows the effect of the supplied heat temperature on the second law efficiency. While the second type of exergy efficiency, $\eta_{II,2}$, monotonically decreases with increasing temperature, the first type efficiency, $\eta_{II,1}$, shows a minimum at around 62°C. Both the input exergy and useful output exergy (exergy of the produced distillate) increase by increasing the hot-end temperature. However, the decreasing trend of $\eta_{II,2}$ suggests that the increase in the exergy of the input thermal energy overweighs the higher exergy of the distillate. The trend of $\eta_{II,1}$ shown in Fig. 21 suggests that there exists a certain heat supply temperature at which the ratio of exergy destruction to the input exergy is maximized.

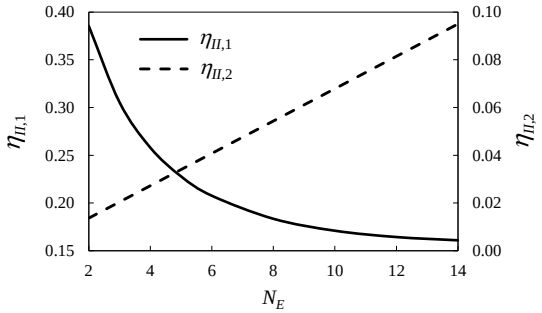

Fig. 22 The variations of the second law efficiencies with the number of stages of the MED system

The effect of the number of stages on the second law efficiencies is shown in Fig. 22. In general, increasing the number of stages (also referred to as *effects*) increases the overall thermal resistance of the system. Since the heat source and heat sink temperatures are fixed, increased thermal resistance results in smaller heat throughput and hence smaller exergy input. Increased thermal resistance also leads to a slight increase in the overall temperature drop and its associated exergy destruction across the system. This results in the decreasing trend of $\eta_{II,1}$ shown in Fig. 22. The smaller heat throughput also implies smaller distillate production rate in each effect. However, the increased number of effects more than offsets the reduced distillation rate in individual effects. As expected, $\eta_{II,2}$ increases due to the decreased heat transfer (smaller input thermal exergy) and increased distillation rate (greater useful output exergy). Overall, MED systems with greater number of effects are more efficient from both energy and exergy points of view. Nevertheless, it should be noted that the improved efficiency comes with higher capital cost associated with higher material and manufacturing costs (Mistry *et al.*, 2013).

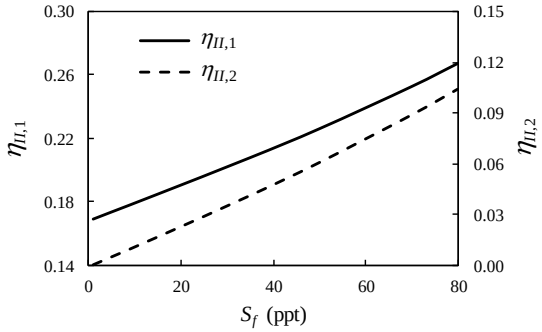

Fig. 23 The variations of the second law efficiencies with the salinity of the input water

Global Digital Central
ISSN: 2151-8629

Effect of salinity of the input water on the second law efficiency is shown in Fig. 23. For a fixed heat source temperature, increased salinity of the feed water slightly increases the overall thermal resistance of the distillation system and hence the heat throughput and corresponding input exergy slightly decrease. Also, as the feed water salinity increases, more work (exergy) will be needed to separate fresh water from it due to the greater difference between the chemical potential of the fresh water and that of the total dead state (feed water). The increase of the specific exergy of the distilled water overweighs the slight decrease in the amount of distilled water production. As such, $\eta_{II,2}$ increases by increasing the feed water salinity. The increasing trend of $\eta_{II,1}$ with the feed water salinity can be explained by the greater output exergy mainly due to the higher exergy of produced distillate and discharging brine. Finally, the effect of non-ideality of the saline water on the second law efficiency is shown in Fig. 24. As evident, the ideal solution assumption leads to an overprediction of $\eta_{II,2}$ compared to the actual solution.

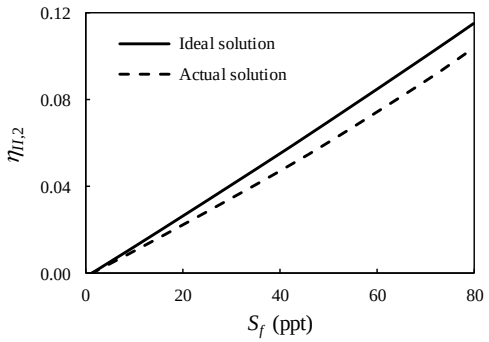

Fig. 24 Comparison between the second law efficiencies based on the ideal solution approximation and actual thermophysical properties

5. CONCLUSIONS

A cohesive and general presentation of the exergy analysis for the energy systems was provided. The presented approach was applied to several engineering systems and processes including fuel cells, latent heat thermal energy storage, heat exchangers and thermal desalination system. The critical role of the exergy analysis in the optimal design of energy systems as well as identification of their actual and theoretical limits of performance was established. It was also shown that for the studied systems the exergy efficiency in some cases has opposite trend to the first law efficiency.

6. ACKNOWLEDGEMENTS

Amir Faghri acknowledges support by the National Science Foundation under Grant No.1744118 to the University of Connecticut. Hamidreza Shabgard acknowledges support from the Gallogly College of Engineering at the University of Oklahoma.

NOMENCLATURE

c_p	specific heat (J/kg·K)
c_p	specific heat at constant pressure (J/kg·K)
c_v	specific heat at constant volume (J/kg·K)
g	gravitational acceleration (m/s^2) or specific Gibbs free energy (J/kg)
g^f	specific Gibbs free energy of formation (J/kg)
h	specific enthalpy (J/kg) or height (m)
h^a	available specific enthalpy or co-enthalpy (J/kg)
h^f	specific enthalpy of formation (J/kg)
M	molar mass (kg/mole) or molarity (number of moles of solute per liter of solution)
m	mass (kg)
$\dot{m}$	mass flow rate (kg/s)
n	number of moles
N_s	entropy generation number
P	pressure (Pa)
P_0	reference pressure (Pa)
Q	thermal energy (J)
$\dot{Q}$	heat transfer rate (W)
q	heat transfer rate (W)
R_g	specific gas constant (J/kg·K)
S	entropy (J/K) or salinity (g/kg aka ppt)
$\dot{S}_{gen}$	entropy generation (W/K)
s	specific entropy (J/kg·K)
s^f	specific entropy of formation (J/kg)
t	time (s)
T	temperature (°C or K)
T_0	reference temperature (K)
$\bar{T}$	temperature normalized by the environment temperature (°C)
U	internal energy (J)
U^a	available internal energy or co-energy (J)
u	specific internal energy (J/kg)
V	velocity (m/s) or volume (m^3)
v	specific volume (m^3/kg)
W	work (J)
$\dot{W}$	power (W)
w	specific work (J/kg) or mass fraction
X	exergy (J)
$\dot{X}$	exergy transfer rate (W)
$\dot{X}_{des}$	exergy destruction rate (W)
x	specific exergy (J/kg) or mole fraction
$x_{w,f,dis}$	dissociated mole fraction of the water in the saline feed water

Greek symbols

ε	heat exchanger effectiveness
η	efficiency
η_I	first law efficiency
η_{II}	second law efficiency
ψ	specific flow exergy (J/kg)
μ	chemical potential (J/mole)
ϑ	Carnot factor

Subscripts

0	reference/environment/at dead state
af	adiabatic flame
b	brine
c	cold
ch	chemical
d	distilled water
des	destroyed
f	saline feed water
h	hot
ig	ideal gas
in	input
im	incompressible material
lm	log mean
max	maximum
out	output
P	reaction product
R	reactant
rev	reversible
s	salt
th	thermal
u	actual
w	water

Acronyms

COP	coefficient of performance

Global Digital Central
ISSN: 2151-8629

GOR	gained-output ration
HV	heating value
NTU	number of transfer units
PCM	phase change material
ppt	part per thousand
RDS	restricted dead state
TDS	total dead state

REFERENCES

Bahrami, H., and Faghri, A., 2011, "Exergy analysis of a passive direct methanol fuel cell," *Journal of Power Sources*, **196**(3), 1191–1204. http://dx.doi.org/10.1016/j.jpowsour.2010.08.087.

Bejan, A., 1996, *Entropy generation minimization : the method of thermodynamic optimization of finite-size systems and finite-time processes*, CRC Press.

Bejan, A., 2006, *Advanced engineering thermodynamics*, John Wiley & Sons.

Blanco, J., Malato, S., Fernández-Ibañez, P., Alarcón, D., Gernjak, W., and Maldonado, M.I., 2009, "Review of feasible solar energy applications to water processes," *Renewable and Sustainable Energy Reviews*, **13**(6–7), 1437–1445. http://dx.doi.org/10.1016/J.RSER.2008.08.016.

BoroumandJazi, G., Saidur, R., Rismanchi, B., and Mekhilef, S., 2012, "A review on the relation between the energy and exergy efficiency analysis and the technical characteristic of the renewable energy systems," *Renewable and Sustainable Energy Reviews*, **16**(5), 3131–3135. http://dx.doi.org/10.1016/J.RSER.2012.02.057.

Çengel, Y.A., Kanoglu, M., and Boles, M.A., 2019, *Thermodynamics: an engineering approach*, McGraw-Hill.

Dinçer, I., and Rosen, M.A., 2012, *EXERGY: energy, environment and sustainable development*, Elsevier Science.

Fallah, M., Siyahi, H., Ghiasi, R.A., Mahmoudi, S.M.S., Yari, M., and Rosen, M.A., 2016, "Comparison of different gas turbine cycles and advanced exergy analysis of the most effective," *Energy*, **116**, 701–715. http://dx.doi.org/10.1016/J.ENERGY.2016.10.009.

Galliani, A., and Pedrocchi, E., 2014, *Analisi exergetica*, Polipress.

Hesselgreaves, J.E., 2000, "Rationalisation of second law analysis of heat exchangers," *International Journal of Heat and Mass Transfer*, **43**(22), 4189–4204. http://dx.doi.org/10.1016/S0017-9310(99)00364-6.

Ibrahim, T.K., Mohammed, M.K., Awad, O.I., Abdalla, A.N., Basrawi, F., Mohammed, M.N., Najafi, G., and Mamat, R., 2018, "A comprehensive review on the exergy analysis of combined cycle power plants," *Renewable and Sustainable Energy Reviews*, **90**, 835–850. http://dx.doi.org/10.1016/J.RSER.2018.03.072.

Kaushik, S.C., Reddy, V.S., and Tyagi, S.K., 2011, "Energy and exergy analyses of thermal power plants: A review," *Renewable and Sustainable Energy Reviews*, **15**(4), 1857–1872. http://dx.doi.org/10.1016/J.RSER.2010.12.007.

Li, X., and Faghri, A., 2011, "Local entropy generation analysis on passive high-concentration DMFCs (direct methanol fuel cell) with different cell structures," *Energy*, **36**(1), 403–414. http://dx.doi.org/10.1016/J.ENERGY.2010.10.024.

Lienhard V, J.H., Mistry, K.H., Sharqawy, M.H., and Thiel, G.P., 2017, "Thermodynamics, exergy, and energy efficiency in desalination systems," *Desalination Sustainability: A Technical, Socioeconomic, and Environmental Approach*, H. A. Arafat, ed.

McClintock, F.A., 1951, "The Design of Heat Exchangers for Minimum Irreversibility," *ASME Annual Meeting*, Paper No. 51-A-108.

Mistry, K.H., Antar, M.A., and Lienhard V, J.H., 2013, "An improved model for multiple effect distillation," *Desalination and Water Treatment*, **51**(4–6), 807–821. http://dx.doi.org/10.1080/19443994.2012.703383.

Mistry, K.H., and Lienhard V, J.H., 2013a, "Generalized least energy of separation for desalination and other chemical separation processes," *Entropy*, **15**(12), 2046–2080. http://dx.doi.org/10.3390/e15062046.

Mistry, K.H., and Lienhard V, J.H., 2013b, "Effect of nonideal solution behavior on desalination of a sodium chloride solution and comparison to seawater," *Journal of Energy Resources Technology*, **135**(4), 042003. http://dx.doi.org/10.1115/1.4024544.

Mistry, K.H., McGovern, R.K., Thiel, G.P., Summers, E.K., Zubair, S.M., and Lienhard, J.H., 2011, "Entropy generation analysis of desalination technologies," *Entropy*, **13**(10), 1829–1864. http://dx.doi.org/10.3390/e13101829.

Moran, M.J., Shapiro, H.N., Boettner, D.D., and Bailey, M.B., 2014, *Fundamentals of Engineering Thermodynamics*, Wiley.

Nayar, K.G., Sharqawy, M.H., Banchik, L.D., and Lienhard V, J.H., 2016, "Thermophysical properties of seawater: A review and new correlations that include pressure dependence," *Desalination*, **390**, 1–24. http://dx.doi.org/10.1016/J.DESAL.2016.02.024.

Pal, R., 2018, "Entropy generation and exergy destruction in flow of multiphase dispersions of droplets and particles in a polymeric liquid," *Fluids*, **3**(1), 19. http://dx.doi.org/10.3390/fluids3010019.

Pavelka, M., Klika, V., Vágner, P., and Maršík, F., 2015, "Generalization of exergy analysis," *Applied Energy*, **137**, 158–172. http://dx.doi.org/10.1016/J.APENERGY.2014.09.071.

Piacentino, A., 2015, "Application of advanced thermodynamics, thermoeconomics and exergy costing to a Multiple Effect Distillation plant: In-depth analysis of cost formation process," *Desalination*, **371**, 88–103. http://dx.doi.org/10.1016/j.desal.2015.06.008.

Sansaniwal, S.K., Sharma, V., and Mathur, J., 2018, "Energy and exergy analyses of various typical solar energy applications: A comprehensive review," *Renewable and Sustainable Energy Reviews*, **82**, 1576–1601. http://dx.doi.org/10.1016/J.RSER.2017.07.003.

Shabgard, H., Bergman, T.L., and Faghri, A., 2013, "Exergy analysis of latent heat thermal energy storage for solar power generation accounting for constraints imposed by long-term operation and the solar day," *Energy*, **60**. http://dx.doi.org/10.1016/j.energy.2013.08.020.

Shabgard, H., Robak, C.W., Bergman, T.L., and Faghri, A., 2012, "Heat transfer and exergy analysis of cascaded latent heat storage with gravity-assisted heat pipes for concentrating solar power applications," *Solar Energy*, **86**(3), 816–830. http://dx.doi.org/10.1016/j.solener.2011.12.008.

Shabgard, H., Song, L., and Zhu, W., 2018, "Heat transfer and exergy analysis of a novel solar-powered integrated heating, cooling, and hot water system with latent heat thermal energy storage," *Energy Conversion and Management*, **175**, 121–131. http://dx.doi.org/10.1016/J.ENCONMAN.2018.08.105.

Sharqawy, M.H., Lienhard V, J.H., and Zubair, S.M., 2010, "Thermophysical properties of seawater: a review of existing correlations and data," *Desalination and Water Treatment*, **16**(1–3), 354–380.

Global Digital Central
ISSN: 2151-8629

http://dx.doi.org/10.5004/dwt.2010.1079.

Torabi, M., Zhang, K., Karimi, N., and Peterson, G.P., 2016, "Entropy generation in thermal systems with solid structures – A concise review," *International Journal of Heat and Mass Transfer*, **97**, 917–931. http://dx.doi.org/10.1016/J.IJHEATMASSTRANSFER.2016.03.007.

Warsinger, D.M., Mistry, K.H., Nayar, K.G., Chung, H.W., and Lienhard V, J.H., 2015, "Entropy generation of desalination powered by variable temperature waste heat," *Entropy*, **17**(11), 7530–7566. http://dx.doi.org/10.3390/e17117530.